Air Plasma Modification of Graphite-Based Electrode for Improved Performance of Aqueous Redox Flow Batteries

Patricia Bassil, Coumba Fall, Karim Boutamine, Frédéric Favier, Steven Le Vot

Air Plasma Modification of Graphite-Based Electrode for Improved Performance of Aqueous Redox Flow Batteries

Journal:	*Journal of The Electrochemical Society*
Manuscript ID	JES-112339.R2
Manuscript Type:	Research Paper
Date Submitted by the Author:	31-May-2024
Complete List of Authors:	Bassil, Patricia; University of Montpellier Faculty of Sciences Fall, Coumba; University of Montpellier Faculty of Sciences Boutamine, Karim; University of Montpellier Faculty of Sciences Favier, Frederic; University of Montpellier Faculty of Sciences, Institut Charles Gerhardt Montpellier UMR 5253 CNRS-UM-ENSCM Le Vot, Steven; University of Montpellier Faculty of Sciences,
Keywords:	Batteries – aqueous, Plasma, Electrode Kinetics

Air Plasma Modification of Graphite-Based Electrode for Improved Performance of Aqueous Redox Flow Batteries

Patricia Bassil,[1,2] Coumba Fall,[1,2] Karim Boutamine,[1,2,3] Frédéric Favier,[1,2] and Steven Le Vot[1,2,z]

[1]ICGM, CNRS, Univ. Montpellier, ENSCM, Montpellier, France
[2]Réseau sur le Stockage Electrochimique de l'énergie (RS2E), FR CNRS 3459, France
[3]Aix-Marseille Université, CNRS, ICR UMR7273, Marseille, France
Steven.le-vot@umontpellier.fr

Abstract
Graphite felt is widely utilized as a porous carbon electrode in aqueous redox flow batteries (RFBs). However, its inherent hydrophobic nature and limited electrochemical activity present challenges. While the correlation between RFB performance and electrode properties has been extensively studied for vanadium chemistry and other inorganic redox active materials, it remains scarce in literature for organic systems. In this study, we employ air plasma treatment, known for its controllability, solvent-free nature, and short treatment duration, to modify commercially available graphite felt for RFB applications. A comprehensive analysis is conducted to establish correlations between plasma treatment, physical properties, electrochemical characteristics, and overall cell performance in aqueous RFBs. Comparative evaluation reveals a significant enhancement, with treated graphite felt exhibiting an 85% increase in capacity at 140 mA cm^{-2} compared to its pristine counterpart. By intentionally utilizing authentic RFB electrodes and employing state-of-the-art ferrocyanide posolyte, this study underscores the crucial role of the interface, even for rapid (reversible) redox-active materials utilized in AORFBs.

1. Introduction

Our society is currently facing an unprecedented energy crisis, necessitating a substantial reduction in greenhouse gas emissions. To achieve this, there is a widespread acknowledgment of the need to significantly decrease fossil fuel consumption, with renewable energies expected to play an increasingly prominent role in the global energy mix. Battery storage is widely recognized as one of the most accessible and efficient solutions to balance supply and demand in this context. Consequently, the stationary energy storage market is experiencing rapid growth. Presently, lead-acid batteries and lithium-ion batteries (LIB) dominate the energy storage market. However, lead-acid batteries are deemed unsuitable for large-scale energy storage due to inherent limitations. Driven by electric vehicle development, lithium-ion

batteries have emerged as the leading technology, offering energy densities surpassing 300 Wh kg^{-1} and costs nearing €100 kWh^{-1}. Despite these advantages, lithium-ion batteries face significant challenges related to safety and material resource concerns.

Redox flow batteries (RFB) are composed of large external tanks containing solubilized redox species and a stack of electrochemical cells in which redox reactions occurs with the electrolyte flowing through carbon felts electrodes[1,2]. RFB are actually a large family of electrochemical devices that have been studied using many chemical configurations (mainy playing with the nature of redox species). As a key advantage over other technologies, RFB decouple power and capacity, offering safety high flexibility for large-scale energy storage. Vanadium RFB (VRFB) is one of the most commercialized long-duration battery technologies but suffers from several major drawbacks (electrolyte imbalance, contamination and cell components corrosion that cause issues regarding long term stability of the system. Nowadays, existing VRFB are in the range of 300 – 800 US$·$kWh^{-1}$. The low solubility (≈ 2 M) of redox moieties combined to the narrow cell voltage (1.2 V) leads to low energy density (< 50 $Wh \cdot L^{-1}$). A further detrimental limitation that is the high and volatile cost of vanadium combined to the fact that this element is listed as a critical raw material, make likely that VRFB may never be a major part of the energy mix.

To offer alternatives to vanadium redox flow batteries (VRFBs), significant efforts have been directed towards the development of aqueous organic redox flow batteries (AORFBs) since the mid-2010s[3–7]. One of the key advantages of employing organic molecules lies in the ability to engage in molecular engineering to tailor the properties of redox-active species, including solubility, redox potential, and stability. While an extensive array of organic compounds has been investigated, the identification of candidates suitable for industrial development remains limited. Summarizing a decade of research, two primary approaches have emerged: 1) AORFBs operating at very high pH levels (13-14) typically utilize quinones for the negative compartment

(negolyte or anolyte) and iron coordination complexes (such as $Fe(CN)_6^{4-}$) for the positive compartment (posolyte or catholyte). It's noteworthy that $Fe(CN)_6^{4-}$ is not an organic molecule. 2) AORFBs operating at close-to-neutral pH levels commonly employ viologen derivatives for the negolyte and nitroxide radicals (or iron coordination complexes, *e.g.*, ferrocene derivatives) for the posolyte.

When examining electrochemistry, a stark contrast emerges between inorganic (primarily vanadium, but also chromium, for example) and organic redox-active materials utilized in RFBs. Inorganic systems tend to exhibit sluggish (irreversible) kinetics, whereas organic counterparts often demonstrate reversibility. It's evident that electrodes (typically porous carbon felts) play a crucial role in determining device performance[8,9]. Electrode properties influence charge transfer, ohmic losses, and mass transport within an RFB. The quality of the interface between the electrode and electrolyte governs the activity, selectivity, and stability of the RFB. Consequently, much of the research effort has been directed towards VRFBs, given their commercially established status and poor kinetics.

There are two primary avenues explored to enhance the performance of carbon electrodes. Firstly, catalyst deposition on carbon fibers is investigated[9,10]. These catalysts must exhibit stability in highly acidic environments, be cost-effective, and exhibit low catalytic activity towards water decomposition reactions. Secondly, introducing oxygenated functional groups onto carbon electrodes to generate active sites and increase hydrophilicity is pursued[11,12] This is typically achieved through thermal and/or acidic treatments, although air plasma and microwave[13] treatments have also been reported[14–21]. In the field of electrochemistry, it is well known that oxides on carbon play a significant role[22,23]. The $Fe(CN)_6^{3-/4-}$ redox couple is sensitive to the state of the carbon electrode, and McCreery classifies this redox couple as "surface sensitive" but not "oxide-dependent"[24]. This means that while oxygenated moieties are required to catalyze the process, the specific chemical nature of these moieties (such as

carbonyls, phenolics, lactones, ethers, or carboxylates) is not critical. However, the role of oxygenated functionalities remains unclear, making it challenging to understand the electrochemical kinetics of flow batteries, even for well-studied ferrocyanide complexes involving only a single electron transfer[25].

In the context of AORFBs, studies addressing electrochemical processes at modified interfaces are relatively scarce[26–28], with research primarily focusing on electrolyte development. Gao *et al.* demonstrated that the electrochemical reversibility and activity of anthraquinone on graphite felt can be significantly enhanced through thermal treatment at 550°C under air, attributing this improvement to the presence of C-OH functional groups[29]. Xia *et al.* showed that heating a carbon felt at 600°C for 2 hours can mitigate capacity loss, resulting in an extended lifetime of quinone-based RFBs[30]. They postulated that oxygenated electrodes inhibit dimerization between two anthrone molecules by re-oxidizing them to the initial dihydroxyanthraquinone state.

In addition to thermal annealing, plasma treatments offer an efficient and controlled means to modify the surface chemistry and structure of the electrode. Despite several reports of such treatments for VRFBs[14–21], only one publication has explored surface modification using plasma for AORFBs[31], focusing on acidic AORFB, which is not the most common medium for AORFBs. In this latter study, Permatasari *et al.* demonstrated that the electron transfer rate of Tiron A was improved thanks to oxygen functional groups formed by O_2 plasma treatments[31].

In this study, we present, for the first time, the impact of air-plasma treatment on the performance of "real" AORFBs. Specifically, we chose to functionalize commercial electrodes (SGL - GFD 4.65 EA) used by RFB companies and assess their electrochemical behavior using state-of-the-art posolyte, *i.e.*, potassium ferrocyanide (pH = 14).

2. Methods

2.1. Plasma treatments

The pristine graphite felt (GF) utilized for plasma treatments was procured from SGL Carbon Co. (GFD 4.65 EA, Germany). Graphite felt samples measuring 6 cm x 6 cm were subjected to air plasma treatment using a plasma generator from Europlasma, which incorporates a 13.56 MHz RF generator (Integro 133 Advanced Energy) with a power rating of 300 W. The graphite felt (SGL 4.65) was introduced into the plasma chamber, which was subsequently evacuated to a pressure below 0.2 mbar before being filled with approximately 0.5 mbar of air. The duration of plasma treatment varied from 2 to 30 minutes on both sides of the electrode. The modified electrodes are denoted as follows: AGF-x, where AGF represents Activated Graphite Felt and x denotes the duration of plasma treatment in minutes (AGF-2, AGF-10, AGF-15, AGF-20, and AGF-30).

2.2. Physical characterization

The morphology of the graphite felt was examined via scanning electron microscopy (SEM) utilizing an FEI Quanta 200 FEG instrument (Source: FEG Schottky). Surface characterization of the electrodes was conducted through X-ray photoelectron spectroscopy (XPS) measurements within the range of 0 to 1200 eV. XPS analyses were performed using the ESCALAB 250 spectrum from Thermo Electron. The monochromatic Al Kα line (1486.6 eV) served as the excitation source. The diameter of the analyzed surface area was 500 µm. Photoelectron spectra were calibrated in binding energy relative to the energy of the C=C component at 284.4 eV. Charge compensation was achieved using a low-energy electron beam

(-2 eV). Data analysis was carried out employing XPSPeak41 software with Shirley background correction.

2.3. Electrochemical characterization

Cyclic voltammetry (CV) experiments were conducted employing a three-electrode configuration cell. The working electrode was constructed using graphite felt with dimensions of 0.283 cm^2 surface area and 4.65 mm thickness, secured within a PVC tube onto a glassy carbon electrode utilized as a current collector. A platinum wire and Ag/AgCl electrode immersed in saturated KCl (0.199 V vs RHE) served as the counter and reference electrodes, respectively.

Electrochemical capacitance measurements were determined via cyclic voltammetry performed in a 1 M sodium chloride solution. The potential range exhibiting a non-Faradaic current response typically spans a 0.4 V potential window centered on the open-circuit potential of the system. CV measurements entailed sweeping the potential across the non-Faradaic region at five different scan rates: 50, 100, 150, 200, and 250 mV s^{-1}.

Cyclic voltammetry (CV) tests using 3 mM potassium ferrocyanide were conducted in 0.1 M sodium chloride aqueous solutions at scan rates of 10 and 50 mV s^{-1}. All measurements were IR drop compensated and recorded using a VMP3 Biologic potentiostat. For electrochemical impedance spectroscopy (EIS), measurements were carried out at 0.3 V vs Ag/AgCl across a frequency range of 100 mHz to 100 kHz with an amplitude of 30 mV.

2.4. Battery performance

The redox flow battery tests were conducted using a custom-built cell obtained from Kemiwatt, equipped with graphite felt electrodes (SGL Carbon SE; square cuboid dimensions of 50 x 50 x 4.65 mm, providing a geometric surface area of 25 cm^2), composite graphite current collectors and a 90 µm cationic Aquivion ion-exchange membrane. The batteries were operated via EC-Lab software, controlling a BioLogic Science Instruments VSP connected to a 10 A current booster (VM3B-10).

The positive electrolyte (posolyte) was prepared by dissolving 0.3 M potassium ferrocyanide in 50 mL of 1 M NaCl solution, while the negative electrolyte (negolyte) was prepared by dissolving 0.3 M potassium ferricyanide in 50 mL of 1 M NaCl solution. Both electrolytes were pumped at a flow rate of 40 mL min^{-1} using a peristaltic pump (verdefelx RS).

Charge-discharge curves were obtained at current densities ranging from 20 to 140 mA cm^{-2}, with charge and discharge voltage cut-offs set at 0.4 and -0.4 V, respectively.

3. Results and discussion

Figure 1 illustrates the textural properties of carbon fibers. These fibers exhibit a random arrangement with no specific orientation, and their diameter is approximately 10 µm. At this level of magnification, regardless of the treatment duration (ranging from 2 to 30 minutes), no visible indications of structural damage were observed following plasma treatment. This observation suggests that the treatment does not adversely affect the material at the microscopic scale. It is important to emphasize that the images presented are representative of various treated carbon felts. Furthermore, examination of felts recovered after plasma treatment revealed that the mechanical integrity of the carbon was maintained, even after the longest treatments (30 minutes in this study).

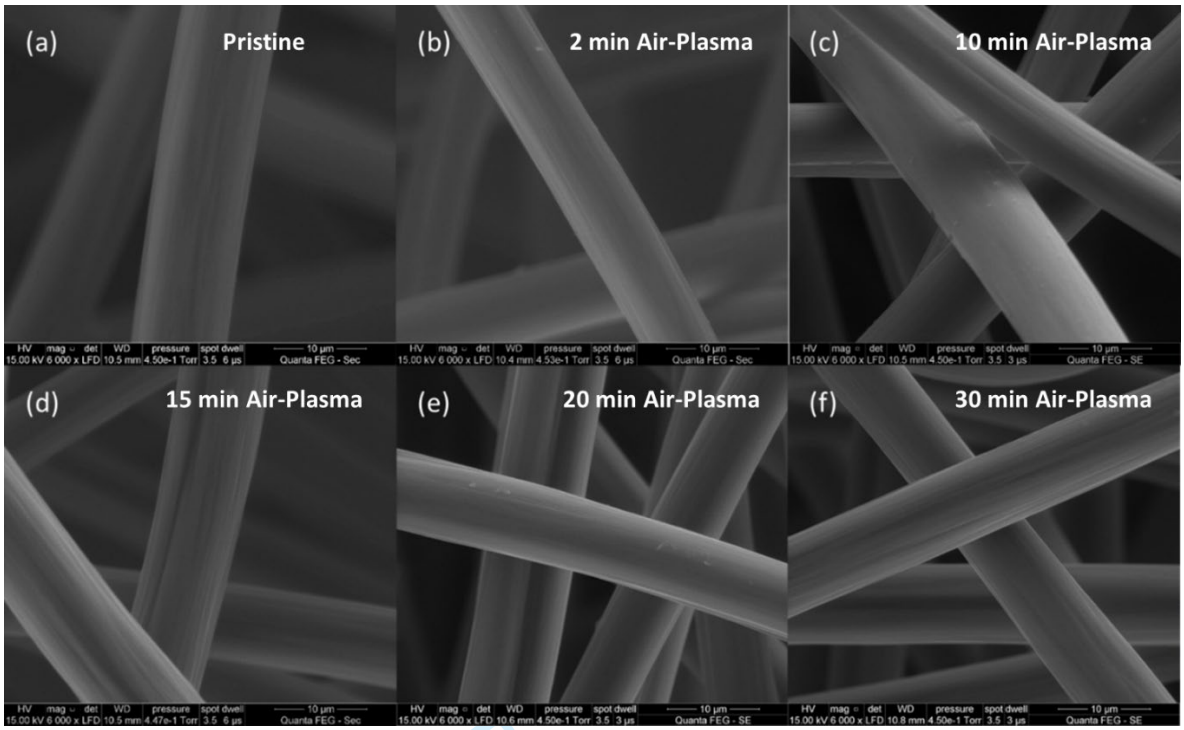

Figure 1: SEM images of a) pristine GF, b) AGF-2, c) AGF-10, d) AGF-15, e) AGF-20 and f) AGF-30

Air plasma treatment is employed to introduce oxygen functionalities onto the surface of the fiber. To verify this, X-ray photoelectron spectroscopy (XPS) was utilized. Figure 2 depicts survey spectra and high-resolution spectra. As anticipated, the analyses confirm the presence of only oxygen and carbon atoms. The intensity of the O1s peak, observed at around 532 eV, is notably low for pristine graphite felt (1.2%), but becomes significant following air plasma modification. The atomic percentages of oxygenated moieties are 8.4%, 9.2%, 7.2%, 9.6%, and 10.8% for treatments of 2, 10, 15, 20, and 30 minutes, respectively. While XPS is recognized as a "semi-quantitative" technique, it is noteworthy that, as a general trend, the oxygen-to-carbon ratio increases with treatment time, albeit to a slight extent.

Given the extensive documentation indicating the significant influence of the precise nature of chemical functionalities on electrochemical activity, this aspect warrants careful consideration.

High-resolution spectra were recorded, and deconvolution of the plasma-treated electrodes is depicted in Figure 2. The analysis reveals the presence of three major components: C=O (531.1 eV), C-OH (532.1 eV), and HO-C=O (533.1 eV)[32]. For each sample, the three functionalities are present, with a predominance of "carboxylic acid" moieties (50 to 60%) compared to "alcohol" (30 to 40%) and "ketone" (10 to 20%). While establishing a direct correlation between plasma treatment duration and the chemical nature of oxygenated functionalities attached to the surface of the carbon fibers should be approached cautiously, it appears that increasing the plasma treatment time promotes the formation of carbonyl groups and decreases the proportion of hydroxyl functions while maintaining a high amount of carboxylic moieties.

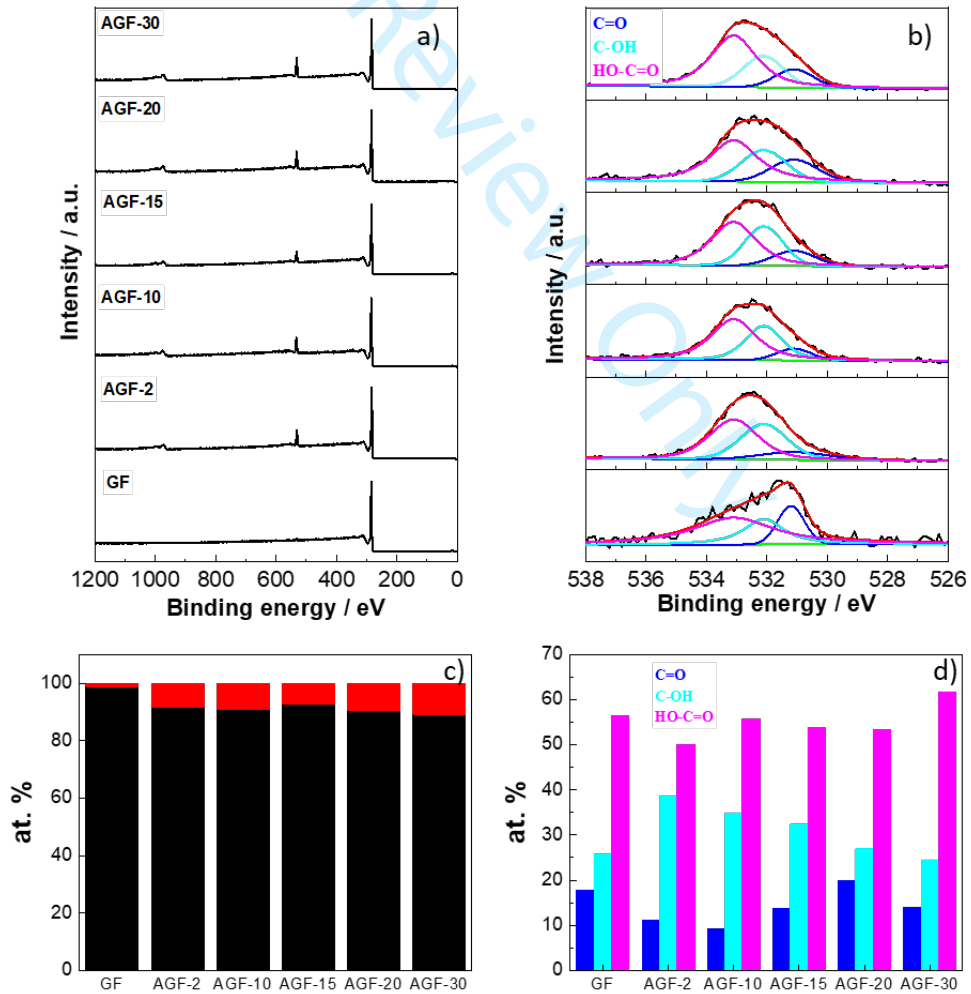

Figure 2: a) XPS Survey, b) high resolution spectra (O1s), c) elemental composition and d) oxygenated moieties proportions for pristine and air-plasma treated graphite felts (AGF-x).

Surface modification can yield two synergistic positive effects. Firstly, hydrophilic oxygenated moieties enhance the wettability of the fibers, thereby improving the electrode/electrolyte interface. Secondly, by altering the electronic density of the carbon, surface modification can catalyze electron transfer during the oxidation and reduction of redox-active materials. To demonstrate the change in hydrophilic character of the fibers, deionized water droplets were deposited on the surfaces of graphite felt (GF), and photographs are presented in Figure 3. A distinct droplet was observed on the surface of pristine GF, exhibiting a high contact angle of approximately 150°. As expected, the surface energy of pristine GF is notably low, indicating poor wettability. In contrast, graphite felts treated with air plasma exhibited immediate absorption of the droplet. In fact, for each modified sample, the droplet was absorbed so rapidly that it was not possible to maintain a stable droplet on the surface of the electrode to measure a contact angle or to capture a relevant picture. It is noteworthy that only a few minutes of solvent-free air treatment are sufficient to achieve the wettability requirement for an RFB carbon electrode.

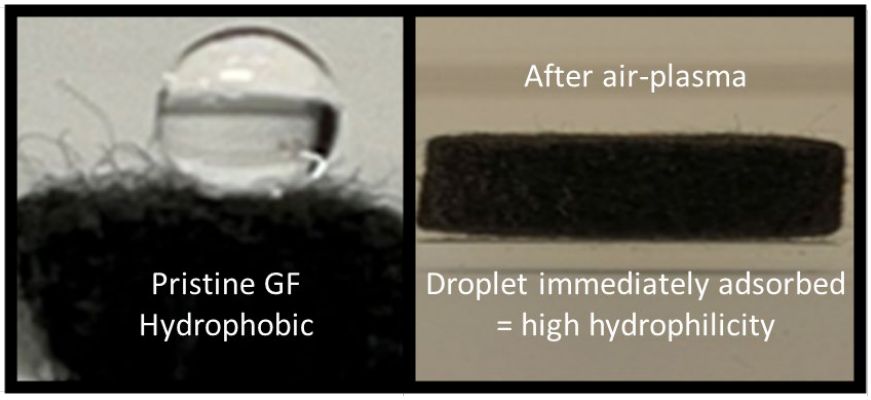

Figure 3: Photographs of the contact angle measurements on pristine and air-plasma treated graphite felt. It was never possible to maintain a droplet on a modified electrode, whatever the air-plasma treatment time.

To gain deeper insights into the influence of plasma treatment on interface properties, the electrochemical capacitances of modified electrodes were investigated. Determining the real electrochemical surface area of porous carbon material presents a challenge. However, an indirect method involves measuring capacitances obtained by integrating cyclic voltammograms obtained at various scan rates in the so-called double layer charging region, as illustrated in Figure 4. As expected for capacitive behavior, a linear relationship between the charge area and scan rate is observed (current is proportional to the scan rate). It is evident that capacitances are significantly increased after plasma treatments, indicating a higher electroactive surface area. This undoubtedly confirms that wettability and thus accessible surface are increased when oxygenated functions are added to the carbon electrodes. Following a 10-minute treatment, the active surface area is seven times higher than that of the pristine graphite felt. It appears that a 2-minute treatment leads to poorer performances, very likely because with this short treatment time, modification cannot occur throughout the thickness (4.6 mm) of the carbon felt. An optimum is reached for treatment times around 10 to 20 minutes.

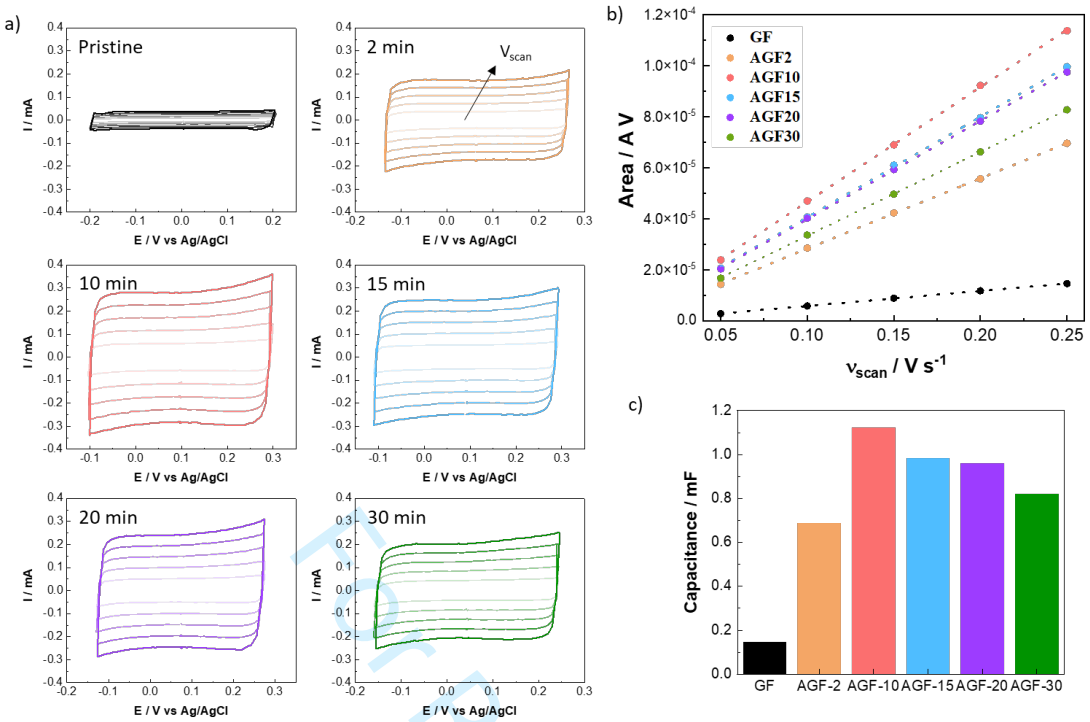

Figure 4: a) Cyclic voltammograms for pristine and air-plasma treated graphite felts recorded in 1 M NaCl aqueous electrolyte. b) Corresponding area for CVs at different scan rates and c) estimated capacitance from these data.

In aqueous organic redox flow batteries (AORFBs), faradaic processes govern current generation. It is anticipated that oxygenated chemical functionalities enhance the wettability of electrodes and improve "intrinsic" kinetics through catalytic effects. The influence of air plasma treatments on the electrochemical performance of graphite electrodes was investigated via cyclic voltammetry in a conventional three-electrode system, utilizing a solution of 3 mM ferrocyanide in 1 M NaCl, as depicted in Figure 5. Ferrocyanide was selected due to its widespread use as a redox probe in electrochemistry, coupled with its current status as the reference posolyte for aqueous organic redox flow batteries[33–35]. The potential separation between the anodic and cathodic peaks provides insights into the reversibility of the redox phenomena occurring on the graphite felt (CVs are corrected for ohmic drop). When utilizing

the pristine felt, due to its poor catalytic activity and/or weak wettability, ferrocyanide does not exhibit any significant redox peaks compared to the modified electrodes. It is evident that the peak potential difference (ΔE) for the $Fe(CN)_6^{3-}/Fe(CN)_6^{4-}$ couple using pristine GF is as large as 1.27 V. This substantial value underscores the sluggishness of the electron transfer on the pristine GF electrode. The peak-to-peak (ΔE) values for modified electrodes are presented in Figure 5, demonstrating that plasma treatments result in lower peak-to-peak separation for each sample. The reduction in peak separation indicates faster kinetic processes. One could also observe that cyclic voltammograms (CVs) no longer exhibit a diffusion-like shape but rather a Gaussian shape. This phenomenon is well-known and corresponds to the CV response when using porous electrodes[36–40]. Interestingly, these findings align with the capacitance data presented in Figure 4. The slight disparities between capacitance measurements and activities concerning a faradic process (ferri/ferro) can be readily explained by the inherent differences in the two physical processes. Finally, another indicator for improved kinetics is that the ratio of the oxidation to reduction current is close to 1 for treated graphite felt but not for pristine GF ($I_{pox} / I_{rirei} = 2.06$), as shown in Figure 5.

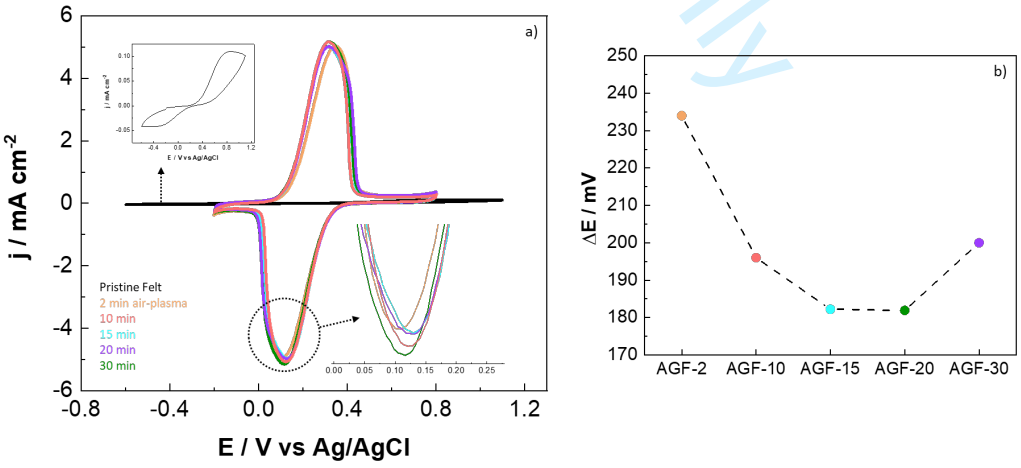

Figure 5: a) Cyclic voltammograms for pristine and air-plasma treated graphite felts recorded in 3 mM $K_4Fe(CN)_6$ and 0.1 M NaCl at 10 mV s^{-1} and b) Corresponding peak potential separation.

For further investigations, electrochemical impedance spectroscopy (EIS) was conducted at 0.3 V vs Ag/AgCl across a frequency range of 100 mHz to 100 kHz, still using an aqueous 3 mM ferrocyanide in 1 M NaCl electrolyte. The Nyquist plots in Figure 6 reveal two semi-circles and one linear part, indicating that the electrochemical reaction on graphite felt is controlled by a combination of kinetic and diffusion processes. The first semi-circle observed at high frequencies is attributed to the contact resistance between fibers[41,42]. The diameter of the second semi-circle corresponds to the charge transfer reaction at the interface between the electrode and the electrolyte, while the slope observed at low frequencies is attributed to diffusion resistance through the pores of the electrode[41,42]. Treated graphite felt exhibits a smaller diameter than pristine GF (Figure 6), indicating lower charge transfer resistance and thus enhanced electrochemical kinetics, which is consistent with the cyclic voltammetry results.

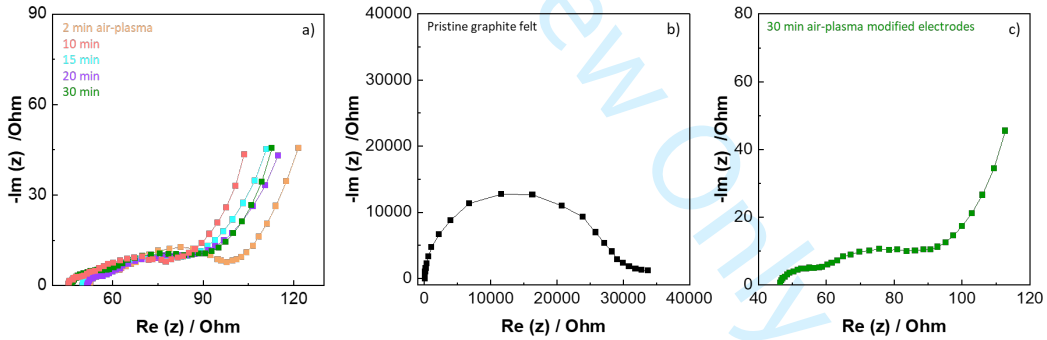

Figure 6: a) Nyquist plots for a) treated and b) pristine graphite felts recorded at 0.3 V vs Ag/AgCl. c) focus on one single diagram to better illustrate the different contributions (two semi circles) discussed in the main text of the publication.

The performance of both pristine and treated graphite felts was investigated in a symmetric redox flow cell[43,44] (25 cm2 – from Kemiwatt RFB company) using various current densities ranging from 20 mA cm^{-2} to 140 mA cm^{-2}. The operating voltage range was set at -0.4 V to 0.4

V. Figure 7 illustrates the charge/discharge profiles of pristine GF and treated AGF-10 for several applied current densities. AGF-10 was selected as the most promising electrode. For the complete set of data, including results for all electrodes and reproducibility assessments, readers are invited to refer to the supplementary information. At low current densities (Figure 7), the difference between modified and pristine electrodes is not significant due to the low polarization of the cell. Interestingly, the gap between the performance of pristine GF and AGF-10 widened gradually with increasing current density. Compared to the pristine graphite felt, utilizing AGF-10 results in reduced charge and discharge overpotentials, as evidenced by the differences in their charge and discharge Nernstian "plateau" potentials. The ohmic losses of the battery assembled with AGF-10 are reduced by 33% at 120 mA cm^{-2}, and the capacity-voltage curves exhibit a relatively higher discharging plateau and lower charging plateau compared to pristine GF. As expected in an RFB, both pristine and treated graphite felts demonstrate a reduction in charge and discharge capacities with increasing current density. However, the RFB cell with AGF-10 electrodes demonstrated enhanced electrolyte utilization, indicating an improved energy density for a given volume of electrolyte. For instance, the discharge capacities of the battery with AGF-10 correspond to 46% and 25% of theoretical capacity at 120 mA cm^{-2} and 140 mA cm^{-2}, respectively. These results represent a 50% and 85% capacity improvement over GF at the respective current densities. Such findings underscore the efficacy of appropriate treatment in enhancing the battery's performance, manifested through reduced polarization, increased capacity, and improved charge transfer rate on the electrode surface.

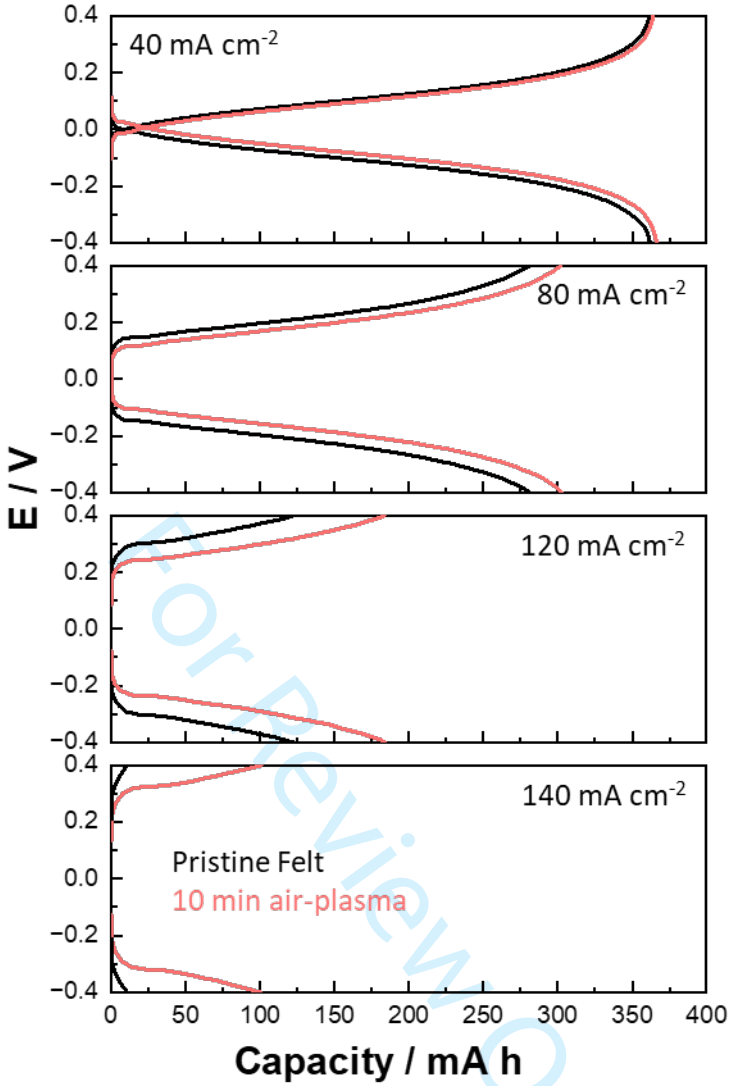

Figure 7: Charge-discharge curves of a symmetric battery assembled with pristine GF and 10 min treated AirGF-10 at the current densities of (a) 40, (b) 80, (c) 120 and (d) 140 mA cm^{-2}

4. Conclusion

The present investigation focuses on assessing the influence of air plasma treatment on augmenting the efficacy of graphite electrodes in aqueous organic redox flow batteries. Plasma treatment presents advantages in terms of simplicity, controllability, and reduced processing time compared to alternative techniques. The treated electrodes exhibited enhanced wettability and heightened electrochemical activity and reversibility in contrast to pristine graphite felt

electrodes. Symmetric redox flow battery tests conducted across various current densities demonstrated the superior performance of graphite felt treated with air plasma for 10 minutes, manifesting an 85% capacity enhancement at 140 mA cm^{-2} compared to pristine graphite felt. Notably, the correlation between AORFB performance and electrode properties has been significantly underestimated in existing literature. By deliberately employing authentic RFB electrodes and employing state-of-the-art ferrocyanide posolyte, we highlight the pivotal role of the interface, even for rapid (reversible) redox-active materials utilized in AORFBs.

Acknowledgments

The authors gratefully acknowledge the French National Research Agency (ANR) for funding this research under the NASTOR program (ANR-21-CE05-0015). The authors also extend their appreciation to Frédéric Fernandez from the Electron and Analytical Microscopy Platform for conducting the SEM experiments, and to Valérie Flaud from the ICGM Technical Platform for assistance with XPS measurements.

References

1. A. G. Olabi, M. A. Allam, M. A. Abdelkareem, T. D. Deepa, A. H. Alami, Q. Abbas, A. Alkhalidi, and E. T. Sayed, *Batteries*, **9**, 409 (2023).

2. M. Park, J. Ryu, W. Wang, and J. Cho, *Nature Reviews Materials*, **2** (2016).

3. J. Winsberg, T. Hagemann, T. Janoschka, M. D. Hager, and U. S. Schubert, *Angewandte Chemie*, **129**, 702–729 (2017).

4. Y. Ding, C. Zhang, L. Zhang, Y. Zhou, and G. Yu, *Chemical Society Reviews*, **47**, 69–103 (2018).

5. D. G. Kwabi, Y. Ji, and M. J. Aziz, *Chemical Reviews*, **120**, 6467–6489 (2020).

6. P. Fischer, P. Mazúr, and J. Krakowiak, *Molecules*, **27**, 560 (2022).

7. F. Zhu, W. Guo, and Y. Fu, *Chem. Soc. Rev.* (2023) https://pubs.rsc.org/en/content/articlelanding/2023/cs/d3cs00703k.

8. A. Forner-Cuenca and F. R. Brushett, *Current Opinion in Electrochemistry*, **18**, 113–122 (2019).

9. R. Wang and Y. Li, *Energy Storage Materials*, **31**, 230–251 (2020).

10. B. Li, M. Gu, Z. Nie, Y. Shao, Q. Luo, X. Wei, X. Li, J. Xiao, C. Wang, V. Sprenkle, and W. Wang, *Nano Lett.*, **13**, 1330–1335 (2013).

11. K. J. Kim, H. S. Lee, J. Kim, M. Park, J. H. Kim, Y. Kim, and M. Skyllas-Kazacos, *ChemSusChem*, **9**, 1329–1338 (2016).

12. W. Zhang, J. Xi, Z. Li, H. Zhou, L. Liu, Z. Wu, and X. Qiu, *Electrochimica Acta*, **89**, 429–435 (2013).

13. X. Wu, H. Xu, P. Xu, Y. Shen, L. Lu, J. Shi, J. Fu, and H. Zhao, *Journal of Power Sources*, **263**, 104–109 (2014).

14. J.-Z. Chen, W.-Y. Liao, W.-Y. Hsieh, C.-C. Hsu, and Y.-S. Chen, *Journal of Power Sources*, **274**, 894–898 (2015).

15. D. Dixon, D. J. Babu, J. Langner, M. Bruns, L. Pfaffmann, A. Bhaskar, J. J. Schneider, F. Scheiba, and H. Ehrenberg, *Journal of Power Sources*, **332**, 240–248 (2016).

16. L. Estevez, D. Reed, Z. Nie, A. M. Schwarz, M. I. Nandasiri, J. P. Kizewski, W. Wang, E. Thomsen, J. Liu, J. Zhang, V. Sprenkle, and B. Li, *ChemSusChem*, **9**, 1455–1461 (2016).

17. Y. Huang, Q. Deng, X. Wu, and S. Wang, *International Journal of Hydrogen Energy*, **42**, 7177–7185 (2017).

18. T. Greese, P. A. Loichet Torres, D. Menga, P. Dotzauer, M. Wiener, and G. Reichenauer, *J. Electrochem. Soc.*, **168**, 070554 (2021).

19. T. Jirabovornwisut, B. Singh, A. Chutimasakul, J.-H. Chang, J.-Z. Chen, A. Arpornwichanop, and Y.-S. Chen, *Materials*, **14**, 3847 (2021).

20. S.-Y. Chen, Y.-L. Kuo, Y.-M. Wang, W.-M. Hsu, T.-H. Chien, C.-F. Lin, C.-H. Kuo, A. Okino, and T.-C. Chiang, *Catalysts*, **11**, 627 (2021).

21. C.-H. Lin, Y.-D. Zhuang, D.-G. Tsai, H.-J. Wei, and T.-Y. Liu, *Polymers*, **12**, 1372 (2020).

22. X. Ji, C. E. Banks, A. Crossley, and R. G. Compton, *ChemPhysChem*, **7**, 1337–1344 (2006).

23. I. Dumitrescu, P. R. Unwin, and J. V. Macpherson, *Chem. Commun.*, 6886 (2009).

24. R. L. McCreery, *Chem. Rev.*, **108**, 2646–2687 (2008).

25. T. V. Sawant and J. R. McKone, *J. Phys. Chem. C*, **123**, 144–152 (2019).

26. H. Agarwal, E. Roy, N. Singh, P. A. A. Klusener, R. M. Stephens, and Q. T. Zhou, *Advanced Science*, **11**, 2307209 (2024).

27. V. Feynerol, R. El Hage, M. Brites Helú, V. Fierro, A. Celzard, L. Liu, and M. Etienne, *Electrochimica Acta*, **421**, 140373 (2022).

28. W. Lee, B. W. Kwon, and Y. Kwon, *ACS Applied Materials and Interfaces*, **10**, 36882–36891 (2018).

29. F. Gao, X. Li, Y. Zhang, C. Huang, and W. Zhang, *ACS Omega*, **4**, 13721–13732 (2019).

30. L. Xia, W. Huo, H. Zhang, K. Xu, Y. Qing, F. Chu, C. Zou, H. Liu, and Z. Tan, *ACS Applied Energy Materials*, **5**, 1984–1991 (2022).

31. A. Permatasari, J. W. Shin, W. Lee, J. An, and Y. Kwon, *International Journal of Energy Research*, **45**, 17878–17887 (2021).

32. H. Radinger, A. Ghamlouche, H. Ehrenberg, and F. Scheiba, *J. Mater. Chem. A*, **9**, 18280–18293 (2021).

33. E. M. Fell, D. D. Porcellinis, Y. Jing, V. Gutierrez-Venegas, T. Y. George, R. G. Gordon, S. Granados-Focil, and M. J. Aziz, *J. Electrochem. Soc.*, **170**, 070525 (2023).

34. X. Li, Y. Yao, C. Liu, X. Jia, J. Jian, B. Guo, S. Lu, W. Qin, Q. Wang, and X. Wu, *Angewandte Chemie International Edition*, **62**, e202304667 (2023).

35. J. Luo, A. Sam, B. Hu, C. DeBruler, X. Wei, W. Wang, and T. L. Liu, *Nano Energy*, **42**, 215–221 (2017).

36. F. G. Chevallier, L. Jiang, T. G. J. Jones, and R. G. Compton, *Journal of Electroanalytical Chemistry*, **587**, 254–262 (2006).

37. D. Menshykau and R. G. Compton, *Langmuir*, **25**, 2519–2529 (2009).

38. K. R. Ward and R. G. Compton, *Journal of Electroanalytical Chemistry*, **724**, 43–47 (2014).

39. T. Tichter, D. Andrae, J. Mayer, J. Schneider, M. Gebhard, and C. Roth, *Phys. Chem. Chem. Phys.*, **21**, 9061–9068 (2019).

40. T. Tichter, J. Schneider, D. Andrae, M. Gebhard, and C. Roth, *ChemPhysChem*, **21**, 428–441 (2020).

41. M. Jing, X. Qi, X. An, X. Ma, D. Fang, X. Fan, J. Liu, and C. Yan, *Electrochimica Acta*, **390**, 138879 (2021).

42. P. C. Ghimire, R. Schweiss, G. G. Scherer, T. M. Lim, N. Wai, A. Bhattarai, and Q. Yan, *Carbon*, **155**, 176–185 (2019).

43. J. D. Milshtein, A. P. Kaur, M. D. Casselman, J. A. Kowalski, S. Modekrutti, P. L. Zhang, N. Harsha Attanayake, C. F. Elliott, S. R. Parkin, C. Risko, F. R. Brushett, and S. A. Odom, *Energy and Environmental Science*, **9**, 3531–3543 (2016).

44. M.-A. Goulet and M. J. Aziz, *J. Electrochem. Soc.*, **165**, A1466 (2018).